RESEARCH PAPER

Pi-shaped quarter wavelength structure for multiband applications

ZHEBIN WANG AND CHAN-WANG PARK

In this paper, for the first time, we present a novel Pi-shaped structure using resonators for multiband applications. The multiband Pi-shaped structure with LC resonators is analyzed. In order to demonstrate the proposed multiband Pi-shaped structure, one tri-band Wilkinson power divider and one tri-band rat-race coupler are designed, fabricated, and tested. The compactness of the two demonstrated components is well kept by putting all stubs with resonators inside the components themselves. Measured results are in good agreement with the simulated results.

I. INTRODUCTION

With the tremendous growth in modern wireless communication systems, multiband operations of components and devices are required for different frequency bands associated with different standards and applications, such as the 0.9/1.8/1.9 GHz global systems for mobile communication systems (GSM) bands, the 1.5 GHz global position system (GPS) band, the 2.5/3.5/5.5 GHz worldwide interoperability microwave access (WiMAX) bands, and the 2.4/5.2/5.8 GHz bands of wireless local area networks (WLAN) [1, 2]. Interoperability and co-existence between multi standards is the main critical issue recently. To satisfy this harsh requirement, multi-frequency band operation of components has increasingly become common.

To be used for multiband communication applications and standards, it is required to develop new type of multiband components and devices. Recently, many researches on multiband applications have been presented, such as multiband filter [3, 4], Wilkinson power divider, and rat-race coupler. Quarter wavelength transmission line (TL) as the basic element used in Wilkinson power divider and rat-race coupler has been studied and developed for dual or tri-band performance. For example, coupled lines [5] and T-type TL [6] have been applied effectively in dual-band Wilkinson power divider; dual-band quarter-wave composite right/left-handed TL (CRLH TL) is presented and applied in rat-race coupler [7, 8]; the C-section together with two TL sections is proposed and synthesized for dual-band rat-race coupler [9]; stepped-impedance microstrip line is employed both for multiband Wilkinson power divider

University of Quebec in Rimouski, Electrical Engineering, 300 Allee des Ursulines, Rimouski, Quebec, G5L3A1, Canada. Phone: 1-4187231986 ext: 1737
Corresponding author:
Z. Wang
Email: eawzbhf@gmail.com

[10] and rat-race coupler [11]. To design a multiband Wilkinson power divider or rat-race coupler, a simple quarter wavelength TL with multiband performance is the key to find out.

Multiband power amplifiers (PAs) have been presented in previous works also [12–17]. In traditional multiband PA, parallel path structure with switches has been used [12]. However, the parallel path structure requires multiple PAs, so the cost of component is multiple and the size of the whole structure is large. To reduce the number of parallel PAs, as a solution, a reconfigurable matching network (MN) concept has been introduced in [12–14]. However, with this technology, switches or electronic tunable elements are required for additional signal control and they may introduce distortions [15]. Because of switch or varactor, the multiband performances of PA are unable to be realized simultaneously. Multiband PA using one transistor and one branch of MN without switches or varactor becomes a major solution for multiband purpose recently [16, 17]. In the Doherty PA, power divider and quarter wavelength TL are the key element to divide power and to transform impedance [18]. For the application of multiband Doherty PA, multiband Wilkinson power divider is required to combine the multiband carrier PA and peaking PA, and multiband quarter wavelength TLs are required to transform impedance at the tail of multiband Doherty PA.

Our objective is to develop the Pi-shaped structure to be used as the quarter wavelength TL at each operating frequency for multiband applications [19]. This work is general in terms of number of the operating frequency bands and can be applied in different classes of microwave circuits, such as Wilkinson power divider, rat-race coupler, and PA. In Section II, we will present the topology and principle of the proposed multiband Pi-shaped structure in detail. One tri-band Wilkinson power divider and one tri-band rat-race coupler with compact size are designed, fabricated, and tested in Section III for the demonstration.

II. ANALYSIS OF MULTIBAND PI-SHAPED STRUCTURE

In this section, the proposed multiband (n-band, $n \geq 3$) Pi-shaped structure will be presented and analyzed. Firstly, the topology and principle of the tri-band ($n = 3$) Pi-shaped structure will be explained in Section II(A). Secondly, in Section II(B), the topology and principle of the multiband (n-band, $n \geq 3$) Pi-shaped structure will be presented.

A) Tri-band Pi-shaped structure

Figure 1(a) shows the topology of the tri-band Pi-shaped structure. Figures 1(b)–1(d) show the equivalent circuit of Fig. 1(a) at frequency f_1, f_2, and f_3, respectively. Figures 1(e)–1(g) show the equivalent TL of Fig. 1(a) at frequency f_1, f_2, and f_3, respectively. Figure 1(h) shows the topologies of Wilkinson power divider and rat-race coupler. In this paper, we choose the operating frequency as $f_1 = 2.5$, $f_2 = 1.5$, and $f_3 = 1$ GHz. The resonator f_1 and f_2 in Fig. 1(a) are designed with the resonant frequency f_1 and f_2, respectively. The analysis procedure of the tri-band Pi-shaped structure is shown below:

1) AT FREQUENCY F_1 (2.5 GHZ)

At frequency f_1, in Fig. 1(a), because the resonator f_1 has the resonant frequency f_1, its impedance at frequency f_1 is infinite ideally. So, input signal f_1 is blocked by the first resonators f_1. Therefore, the tri-band Pi-shaped structure shown in Fig. 1(a) will become the equivalent circuit as shown in Fig. 1(b) at frequency f_1. The length and characteristic impedance of the equivalent circuit (Fig. 1(b)) are l_1 and Z_1. At frequency f_1, the equivalent circuit will be used as the quarter wavelength branch in Wilkinson power divider and rat-race coupler as shown in Fig. 1(h), so l_1 is equal to $\lambda_1/4$ and Z_1 is equal to 70.7 Ω.

2) AT FREQUENCY F_2 (1.5 GHZ)

At frequency f_2, an input signal f_2 is passing through the resonator f_1, after then it is blocked by the resonator f_2. Therefore the tri-band Pi-shaped structure will be the equivalent circuit as shown in Fig. 1(c). The length and characteristic impedance of the open-circuited stubs of the equivalent circuit (Fig. 1(c)) are l_2 and Z_2. As mentioned in Section II(A)(1), for the operating frequency f_1 (2.5 GHz), $l_1 = \lambda_1/4$, $Z_1 = 70.7 \,\Omega$. By setting the initial value of Z_2 as 50 Ω at frequency f_2, the ABCD matrix of the equivalent circuit (Fig. 1(c)) will be as the following equation:

$$
\begin{bmatrix} A_2 & B_2 \\ C_2 & D_2 \end{bmatrix} = \begin{bmatrix} 1 & 0 \\ jY_2 \tan(\beta_2 l_2) & 1 \end{bmatrix}
$$
$$
\cdot \begin{bmatrix} \cos(\beta_2 l_1) & jZ_1 \sin(\beta_2 l_1) \\ jY_1 \sin(\beta_2 l_1) & \cos(\beta_2 l_1) \end{bmatrix}
$$
$$
\cdot \begin{bmatrix} 1 & 0 \\ jY_2 \tan(\beta_2 l_2) & 1 \end{bmatrix}
$$
$$
= \begin{bmatrix} \cos(\beta_2 l_1) - Y_2 Z_1 \tan(\beta_2 l_2) \sin(\beta_2 l_1) \\ j2Y_2 \tan(\beta_2 l_2) \cos(\beta_2 l_1) + jY_1 \sin(\beta_2 l_1) \\ -jY_2^2 Z_1 \tan^2(\beta_2 l_2) \sin(\beta_2 l_1) \end{bmatrix}
$$
$$
jZ_1 \sin(\beta_2 l_1)
$$
$$
\cos(\beta_2 l_1) - Y_2 Z_1 \tan(\beta_2 l_2) \sin(\beta_2 l_1) \Bigg],
$$

(1)

where $\beta_2 = \dfrac{2\pi}{\lambda_2}$, $Z_1 = 70.7[\Omega]$, $l_1 = \dfrac{\lambda_1}{4}$, $Z_2 = 50[\Omega]$.

At frequency f_2, the equivalent TL of Fig. 1(a) will be as shown in Fig. 1(f). To be used as a branch of Wilkinson power divider and rat-race coupler as shown in Fig. 1(h),
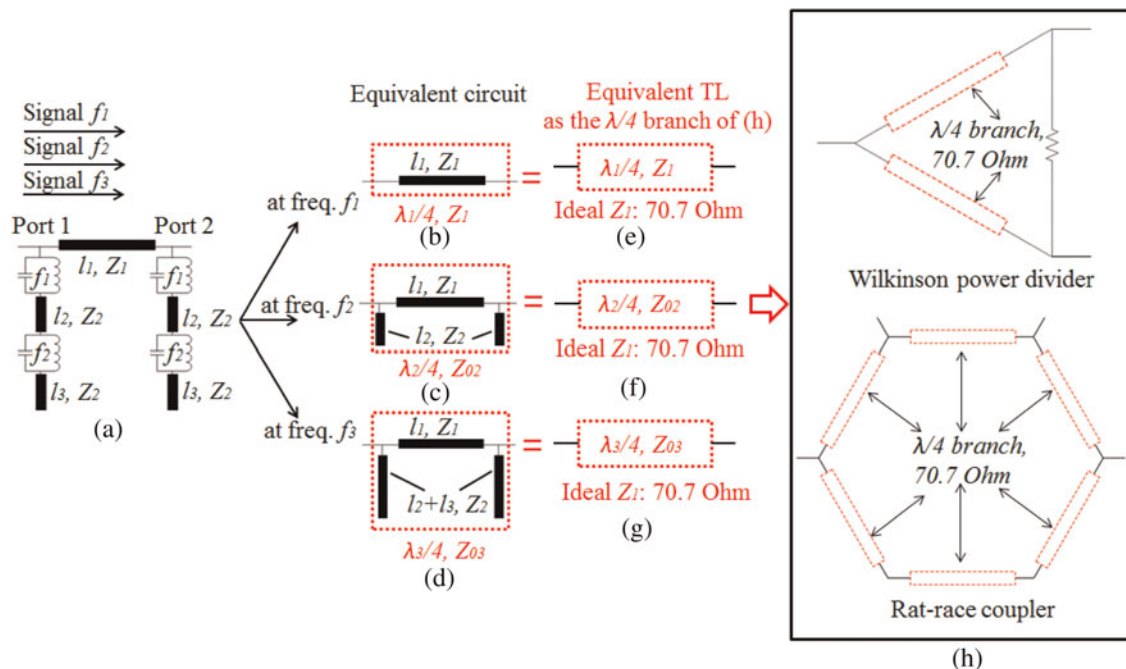

Fig. 1. The principle of the tri-band Pi-shaped structure: (a) the topology of the tri-band Pi-shaped structure, (b–d) the equivalent circuit of (a), (e–g) the equivalent TL of (a), (h) the topologies of Wilkinson power divider and rat-race coupler.

the ideal length and characteristic impedance (Z_{o2}) of the equivalent TL should be $\lambda_2/4$ and 70.7 Ω at frequency f_2. The ABCD matrix of the equivalent TL, which has quarter wavelength at frequency f_2 can be expressed as:

$$\begin{bmatrix} A_2 & B_2 \\ C_2 & D_2 \end{bmatrix} = \begin{bmatrix} 0 & jZ_{o2} \\ jY_{o2} & 0 \end{bmatrix}. \quad (2)$$

In order to calculate the length l_2 shown in Fig. 1(c) and the characteristic impedance Z_{o2} of the equivalent TL shown in Fig. 1(f), we equalize equations (1) and (2) and we can deduce:

$$\Rightarrow Z_1 \tan (\beta_2 l_1) = Z_2 \cot (\beta_2 l_2), \quad (3)$$

$$\Rightarrow Z_{o2} = Z_1 \sin (\beta_2 l_1). \quad (4)$$

At frequency f_2 (1.5 GHz), the characteristic impedance Z_{o2} of the equivalent TL (Fig. 1(f)) is obtained as 57.19 Ω by using equation (4). To use this equivalent TL as a quarter wavelength branch of Wilkinson power divider and rat–race coupler, the ideal value of Z_{o2} should be 70.7 Ω. To increase the value of Z_{o2} up to 70.7 Ω instead of 57.19 Ω, we need to increase Z_1 according to equation (4). But Z_1 has already been determined for frequency f_1, so it should be compromise by doing trade-off between Z_1 and Z_{o2} to satisfy both frequency f_1 and f_2. After fixing the values of Z_1, β_2, l_1, and Z_2, the value of l_2 can be calculated using equation (3).

3) AT FREQUENCY F_3 (1 GHZ)
At frequency f_3, input signal f_3 can pass through the resonator f_1 and resonator f_2. The tri-band Pi-shaped structure shown in Fig. 1(a) becomes the equivalent circuit as shown in Fig. 1(d). The ABCD matrix of the equivalent circuit at frequency f_3 will be as equation (5), where the values of Z_1 and l_1 are as 70.7 Ω and $\lambda_1/4$, those are already determined in Section II(A)(1). The initial value of Z_2 has been given in Section II(A)(2) as 50 Ω.

$$\begin{bmatrix} A_3 & B_3 \\ C_3 & D_3 \end{bmatrix} = \begin{bmatrix} 1 & 0 \\ jY_2 \tan (\beta_3(l_2 + l_3)) & 1 \end{bmatrix}$$
$$\cdot \begin{bmatrix} \cos (\beta_3 l_1) & jZ_1 \sin (\beta_3 l_1) \\ jY_1 \sin (\beta_3 l_1) & \cos (\beta_3 l_1) \end{bmatrix}$$
$$\cdot \begin{bmatrix} 1 & 0 \\ jY_2 \tan (\beta_3(l_2 + l_3)) & 1 \end{bmatrix}$$
$$= \begin{bmatrix} \cos (\beta_3 l_1) - Y_2 Z_1 \tan (\beta_3(l_2 + l_3)) \sin (\beta_3 l_1) \\ j2Y_2 \tan (\beta_3(l_2 + l_3)) \cos (\beta_3 l_1) + jY_1 \sin (\beta_3 l_1) \\ -jY_2^2 Z_1 \tan^2 (\beta_3(l_2 + l_3)) \sin (\beta_3 l_1) \end{bmatrix}$$
$$jZ_1 \sin (\beta_3 l_1)$$
$$\cos (\beta_3 l_1) - Y_2 Z_1 \tan (\beta_3(l_2 + l_3)) \sin (\beta_3 l_1) \end{bmatrix}, \quad (5)$$

where $\beta_3 = \dfrac{2\pi}{\lambda_3}$, $Z_1 = 70.7 [\Omega]$, $l_1 = \dfrac{\lambda_1}{4}$, $Z_2 = 50 [\Omega]$.

At frequency f_3, the equivalent TL of Fig. 1(a) is shown in Fig. 1(g). To be used as a branch of Wilkinson power divider

and rat-race coupler at frequency f_3, the ideal length and characteristic impedance (Z_{o3}) of Fig. 1(g) should be $\lambda_3/4$ and 70.7 Ω. The equivalent TL with quarter wavelength at frequency f_3 can be expressed as:

$$\begin{bmatrix} A_3 & B_3 \\ C_3 & D_3 \end{bmatrix} = \begin{bmatrix} 0 & jZ_{o3} \\ jY_{o3} & 0 \end{bmatrix}. \quad (6)$$

By equalizing (5) and (6), we get

$$\Rightarrow Z_1 \tan (\beta_3 l_1) = Z_2 \cot (\beta_3(l_2 + l_3)), \quad (7)$$

$$\Rightarrow Z_{o3} = Z_1 \sin (\beta_3 l_1). \quad (8)$$

At frequency f_3 (1 GHz), the characteristic impedance Z_{o3} of the equivalent TL in Fig. 1(g) is calculated as 41.56 Ω using equation (8). For the Wilkinson power divider and rat-race coupler application, the idea value of Z_{o3} is 70.7 Ω. So we need to increase the value of Z_{o3} up to 70.7 Ω. To do that, the compromise between Z_{o3} and Z_1 should be made in equation (8). By fixing Z_1, β_3, l_1, and Z_2, the length of the open-circuited stub ($l_2 + l_3$) in Fig. 1(d) can be calculated by equation (7).

As analyzed before, at each operating frequency the tri-band Pi-shaped structure (Fig. 1(a)) is equal to the quarter wavelength TL (Figs 1(e)–1(g)). So we can apply the tri-band Pi-shaped structure (Fig. 1(a)) as a quarter wavelength branch (Fig. 1(h)) in the power divider and coupler. In addition, l_1 is the length of the tri-band Pi-shaped structure (Fig. 1(a)), so it determines the length of the branch of the power divider and coupler. To reduce the size of the components, we set l_1 equal to the quarter wavelength of the highest operating frequency. As mentioned before, frequency f_1 is 2.5 GHz. By equation (3), by fixing the values of Z_1, l_1, and Z_2, the lower frequency f_2 is, the longer the stub length l_2 (Fig. 1(c)) will be. Because the stub length l_2 at frequency f_2 (Fig. 1(c)) is shorter than the stub length ($l_2 + l_3$) at frequency f_3 as shown in Fig. 1(d), we have to choose that the frequency f_3 (1 GHz) is lower than the frequency f_2 (1.5 GHz).

The used substrate in this paper is TLX-8 of TACONIC with dielectric constant 2.55 and dielectric thickness 31 mil. For more precise simulation, the highly accurate, scalable measurement-based chip capacitor and chip inductor models of Modelithics Inc. are used. For microstrip applications, the measured models take into account substrate related parasitic effects and effective series resistance (ESR). With the same capacitance and inductance value for the same resonant frequency, the simulated results of the LC resonators using the ideal (parasitic free) component models and the measurement-based component models of Modelithics Inc. are compared in Fig. 2. We can also use electrically narrow microstrip TL (MTL)-type inductor instead of using chip inductor in the LC resonator. The LC resonator composed of chip inductor and chip capacitor has the advantage of compact size and simple design structure. However, the standard values of the components are limited by the manufactures. For the selected components (the measured models of Modelithics, capacitor model: CAP-ATC-0603-101, 0.1 to 100 pF; inductor model: IND-CLC-0603-102, 1.8–390 nH), the resonant frequency range of the LC resonator is 0.02–8.16 GHz. Parallel LC resonator composed of MTL-type inductor and chip capacitor can avoid the limitation of standard value of lumped element
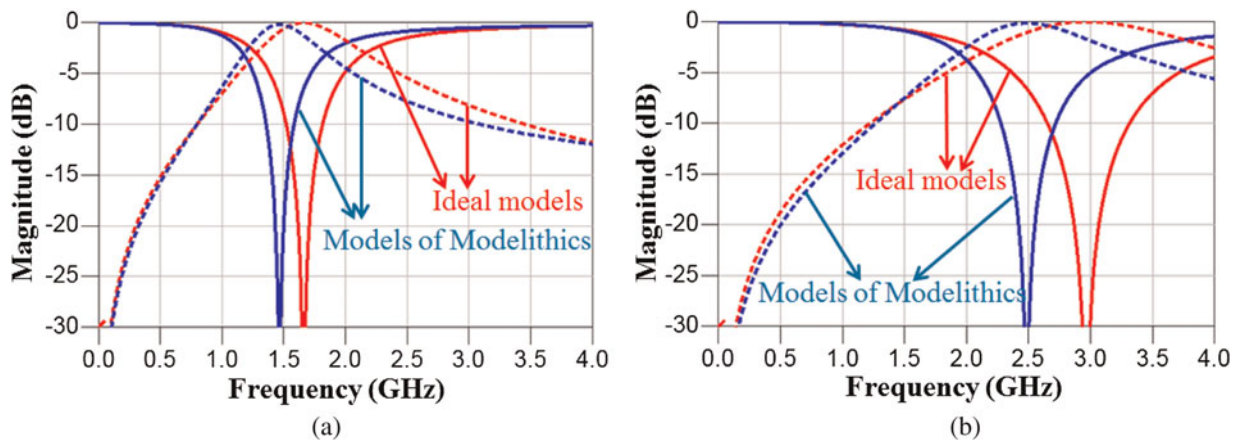
Fig. 2. Simulated comparison of the LC resonators designed by using the ideal models and the measured models of Modelithics Inc. with the same value of capacitance and inductance at (a) 1.5 GHz and (b) 2.5 GHz. Solid line, insertion loss; dot, return loss.

provided by the manufacturers and it can reduce the parasitic effect of chip inductor. In this paper, we use the LC resonator composed of chip capacitor and chip inductor for the tri-band Wilkinson power divider, and use the LC resonator composed of chip capacitor and MTL-type inductor for the tri-band rat-race coupler to demonstrate our proposed multiband design method.

In Advanced Design System (ADS) simulation, the optimized simulation parameters of the tri-band Pi-shaped structure (Fig. 1(a)) are shown in Table 1.

The simulated phase result of the tri-band Pi-shaped structure is shown in Fig. 3. At 1, 1.5, and 2.5 GHz, the S_{21} phase of the tri-band Pi-shaped structure (Fig. 1(a)) is $-89.93°$, $-89.92°$, and $-90.10°$, respectively.

The simulated result of impedance of the tri-band Pi-shaped structure is shown in Fig. 4. The normalized impedance of the Smith chart is 70.7 Ω. At 1.5 GHz, with the load of 70.7 Ω at Port 2 in Fig. 1(a), the impedance at Port 1 (Fig. 1(a)) of the tri-band Pi-shaped structure is 72.8 Ω, whereas the compromised impedances are 36.8 and 135.7 Ω at 1 and 2.5 GHz, respectively. Because the tri-band Pi-shaped structure is equal to the quarter wavelength TL at 1/1.5/2.5 GHz as shown in Fig. 3, the characteristic impedance of the tri-band Pi-shaped structure can be calculated using the single-section quarter-wave matching transformer equation [20] as 51.0/71.8/98.0 Ω at 1/1.5/2.5 GHz, respectively.

The simulated result of insertion loss S_{21} and return loss S_{11} of the tri-band Pi-shaped structure is shown in Fig. 5. At the three operating frequencies 1/1.5/2.5 GHz, the insertion loss is less than 0.64 dB and the return loss is better than 10.02 dB.

B) Multiband (*n*-band, $n \geq 3$) Pi-shaped structure

Right now we do a generalization of the multiband (*n*-band, $n \geq 3$) Pi-shaped structure. The topology of the multiband

Pi-shaped structure is shown in Fig. 6(a). For the *n*-band ($n \geq 3$) Pi-shaped structure, the number of the resonators in the open-circuited stub at each side is $n - 1$. The resonator $f_x(x = 1, \ldots,$ and $n - 1)$ in Fig. 6(a) is used to block frequency f_x while other frequency can pass through it. At frequency f_1 and f_2, as discussed in Section II(A), the equivalent circuit of the multiband Pi-shaped structure is shown in Fig. 6(b) and (c), respectively. At frequency $f_n(n \geq 3)$, the equivalent circuit of Fig. 6(a) is shown in Fig. 6(d). The total length of the open-circuited stub at frequency f_n is equal to $(l_2 + \ldots + l_n)$ with a characteristic impedance of Z_2.

The ABCD matrix of the equivalent circuit at frequency f_n (Fig. 6(d)) is shown as equation (9). As discussed in Section II(A), for the Wilkinson power divider and rat-race coupler applications, we set $Z_1 = 70.7$ Ω and $l_1 = \lambda_1/4$ for frequency f_1. The initial value of Z_2 is given as 50 Ω.

$$
\begin{bmatrix} A_n & B_n \\ C_n & D_n \end{bmatrix} = \begin{bmatrix} 1 & 0 \\ jY_2\tan(\beta_n(l_2+\cdots+l_n)) & 1 \end{bmatrix}
$$
$$
\cdot \begin{bmatrix} \cos(\beta_n l_1) & jZ_1\sin(\beta_n l_1) \\ jY_1\sin(\beta_n l_1) & \cos(\beta_n l_1) \end{bmatrix}
$$
$$
\cdot \begin{bmatrix} 1 & 0 \\ jY_2\tan(\beta_n(l_2+\cdots+l_n)) & 1 \end{bmatrix}
$$
$$
= \begin{bmatrix} \cos(\beta_n l_1) - Y_2 Z_1 \tan(\beta_n(l_2+\cdots+l_n))\sin(\beta_n l_1) \\ j2Y_2\tan(\beta_n(l_2+\cdots+l_n))\cos(\beta_n l_1) + jY_1\sin(\beta_n l_1) \\ -jY_2^2 Z_1\tan^2(\beta_n(l_2+\cdots+l_n))\sin(\beta_n l_1) \end{bmatrix}
$$
$$
jZ_1\sin(\beta_n l_1)
$$
$$
\cos(\beta_n l_1) - Y_2 Z_1\tan(\beta_n(l_2+\cdots+l_n))\sin(\beta_n l_1) \Bigg],
$$
(9)

where $\beta_n = \dfrac{2\pi}{\lambda_n}$, $Z_1 = 70.7 [\Omega]$, $l_1 = \dfrac{\lambda_1}{4}$, $Z_2 = 50 [\Omega]$.

Table 1. Optimized simulation parameters of the tri-band Pi-shaped structure in ADS.

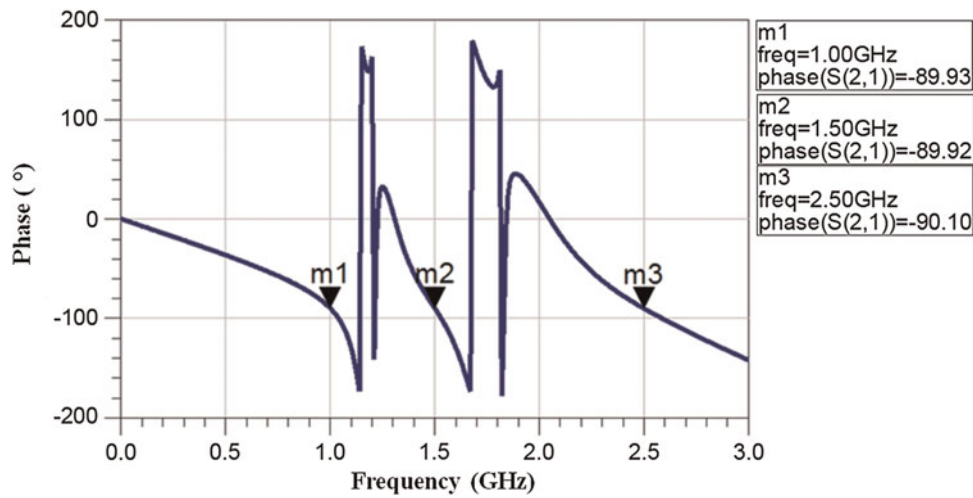| l_1 (mil)	l_2 (mil)	l_3 (mil)	Resonator f_1 LC model of Modelithics	Resonator f_2 LC model of Modelithics
678	96	241	3.6 nH CLC0603CS 0.8 pF ATC600S	5.1 nH CLC0603CS 1.8 pF ATC600S

Fig. 3. The simulated result of phase of the tri-band Pi-shaped structure.

At frequency f_n, the ABCD matrix of the equivalent quarter wavelength TL (Fig. 6(g)) can be expressed as:

$$\begin{bmatrix} A_n & B_n \\ C_n & D_n \end{bmatrix} = \begin{bmatrix} 0 & jZ_{on} \\ jY_{on} & 0 \end{bmatrix}. \qquad (10)$$

For Wilkinson power divider and rat-race coupler, ideally the equivalent length of the equivalent circuit (Fig. 6(d)) should be $\lambda_n/4$ at frequency f_n. To do that, by equalizing equations (9) and (10), it is deduced:

$$\Rightarrow Z_1 \tan(\beta_n l_1) = Z_2 \cot(\beta_n(l_2 + \cdots + l_n)), \qquad (11)$$

$$\Rightarrow Z_{on} = Z_1 \sin(\beta_n l_1). \qquad (12)$$

At frequency f_n, the equivalent characteristic impedance Z_{on} should be approached 70.7 Ω for Wilkinson power divider and rat-race coupler by trading off between Z_{on} and Z_1 using equation (12). By fixing the value of Z_1, β_n, l_1, and Z_2,

the length of the open-circuited stub $(l_2 + \ldots + l_n)$ can be obtained with equation (11).

III. FABRICATION AND MEASUREMENT

A) Tri-band Wilkinson power divider

To demonstrate the proposed multiband design method, by using multiband Pi-shaped structure in Section II, we fabricated one tri-band Wilkinson power divider. The topology and fabricated circuit of the tri-band Wilkinson power divider are shown in Fig. 7. To reduce the size of the circuit, we put all stubs inside the tri-band Wilkinson power divider itself.

The LC resonators f_1 and resonators f_2 in Fig. 7 are composed of chip capacitor and chip inductor. The ideal resonant frequency of LC resonator can be calculated using equation (13), where f_o is the resonant frequency, L is the inductance of inductor, and C is the capacitance of capacitor. The resonant frequency (f_o) of LC resonator increases or decreases while the
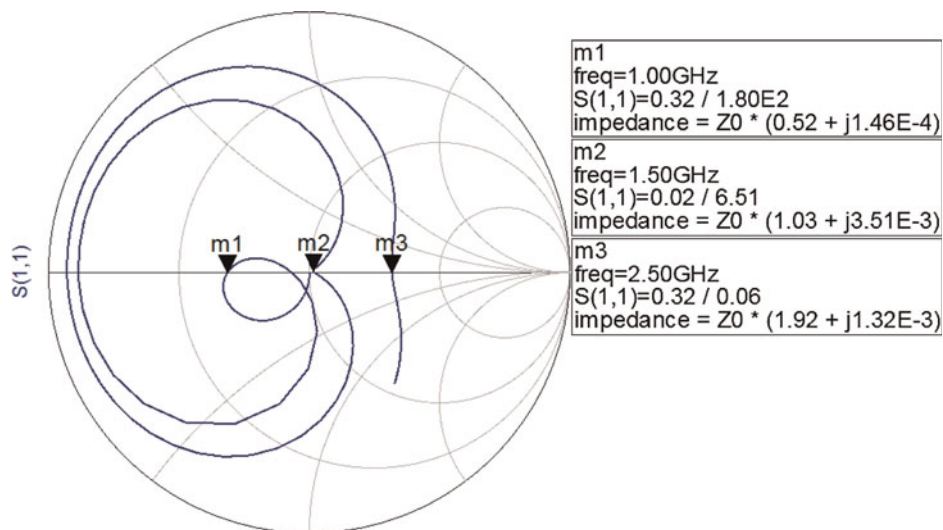

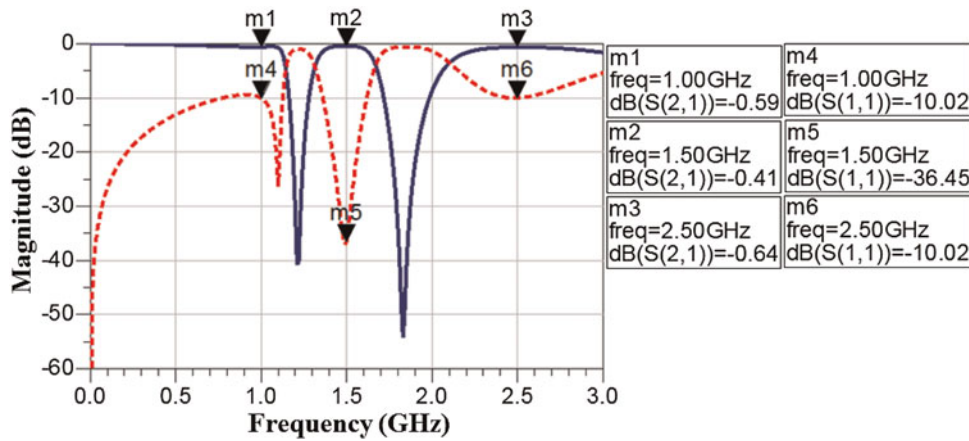**Fig. 4.** The simulated result of impedance of the tri-band Pi-shaped structure.

Fig. 5. The simulated result of insertion loss (solid line) and return loss (dot) of the tri-band Pi-shaped structure.

product of L and C decreases or increases. The resonator f_1 in Fig. 7 has the resonant frequency of 2.5 GHz. As shown in Table 1, the initial capacitance value of the used ATC capacitor model of Modelithics Inc. for the resonator f_1 is 0.8 pF. Figure 8 shows the simulated comparison of the tri-band Wilkinson power divider by only changing the capacitance value of the capacitors in the resonators f_1 in Fig. 7. Because the capacitance value of the resonators f_1 reduces, the highest operating frequency band (2.5 GHz) shifts to a higher frequency band region. To increase the bandwidth of the middle operating frequency band (1.5 GHz) and have a better performance at 2.5 GHz, we reduced the capacitance value of the capacitor models in the resonators f_1 from 0.8 to 0.4 pF as shown in Fig. 8. Figure 9 shows the simulated comparison of the tri-band Wilkinson power divider by only changing the capacitance value of the capacitors in the resonators f_2 in Fig. 7.

Because the resonator f_2 has a resonant frequency of 1.5 GHz, it affects the middle operating frequency band (1.5 GHz). As shown in Fig. 9, the middle operating frequency band (1.5 GHz) shifts to be higher and the bandwidth of the lowest operating frequency band (1 GHz) increases when the capacitance value in the resonators f_2 reduces. The final used capacitance and inductance value in the resonators f_1 and resonators f_2 for the tri-band Wilkinson power divider is 0.4 pF and 3.6 nH, and 1.8 pF and 5.1 nH, respectively.

$$f_0 = \frac{1}{2\pi\sqrt{LC}}. \tag{13}$$

The simulated and measured results of the tri-band Wilkinson power divider are compared from Figs 10–13.
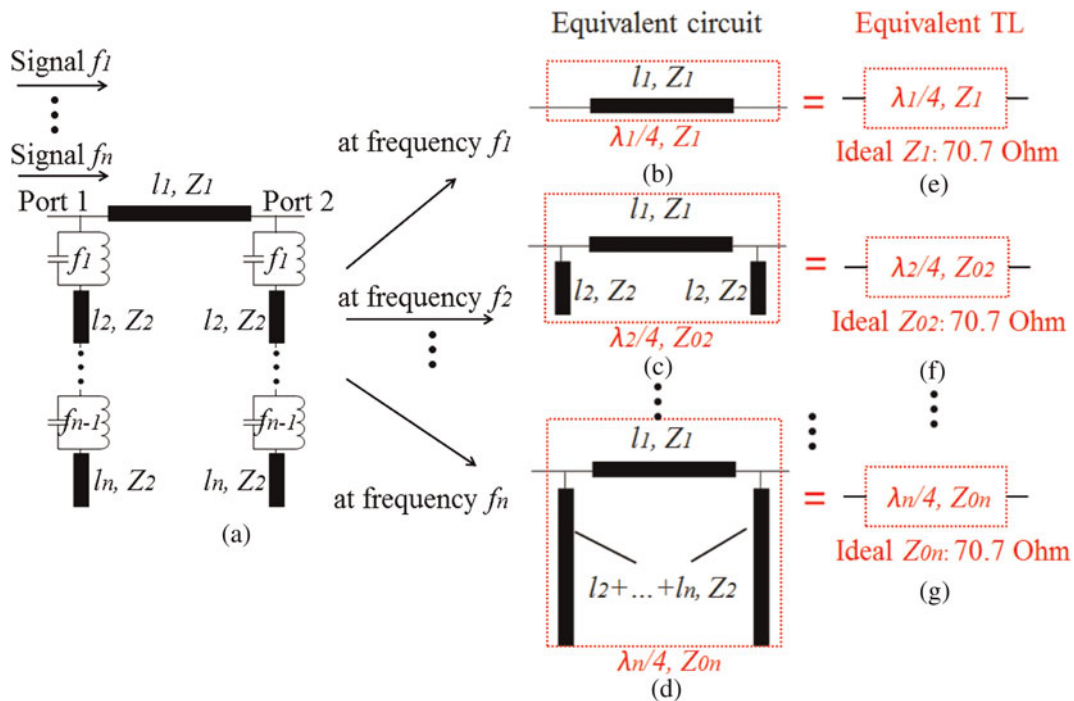

Fig. 6. The principle of the multiband (n-band, $n \geq 3$) Pi-shaped structure: (a) the topology of the multiband Pi-shaped structure, (b–d) the equivalent circuit of (a), (e–g) the equivalent TL of (a).
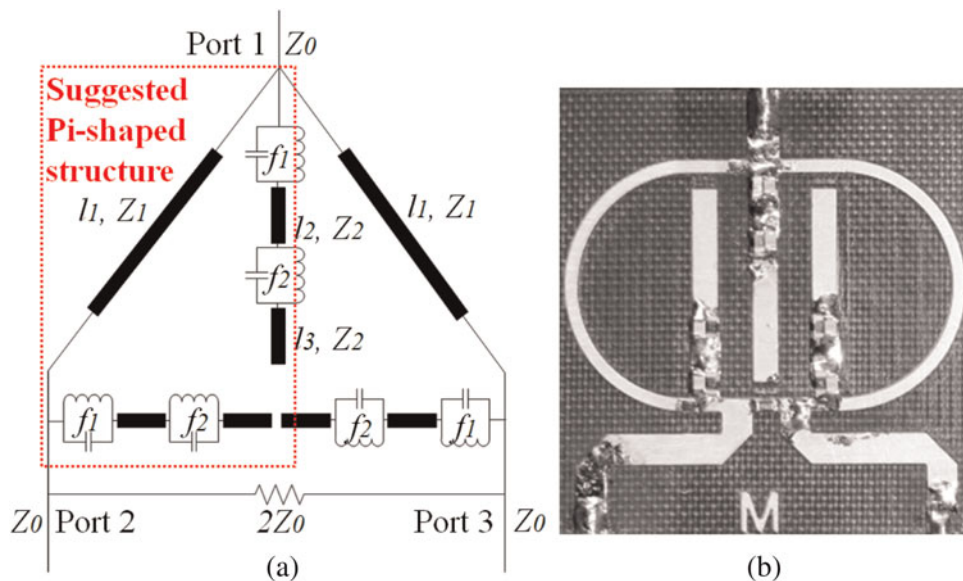
Fig. 7. The topology (a) and fabricated circuit (b) of the tri-band Wilkinson power divider.

The measured insertion loss at $1/1.5/2.5$ GHz is less than 3.78 dB, input and output return loss is more than 12.29 dB, and output isolation is better than 19.93 dB. The simulated results are consistent with the measured results. The measured

phase difference between the two output ports is less than $2.1°$ as shown in Fig. 24 (solid line).

In Fig. 10, the measured insertion loss S_{21} and S_{31} at $1/1.5/2.5$ GHz is $3.58/3.64/3.78$ and $3.59/3.64/3.74$ dB, respectively.
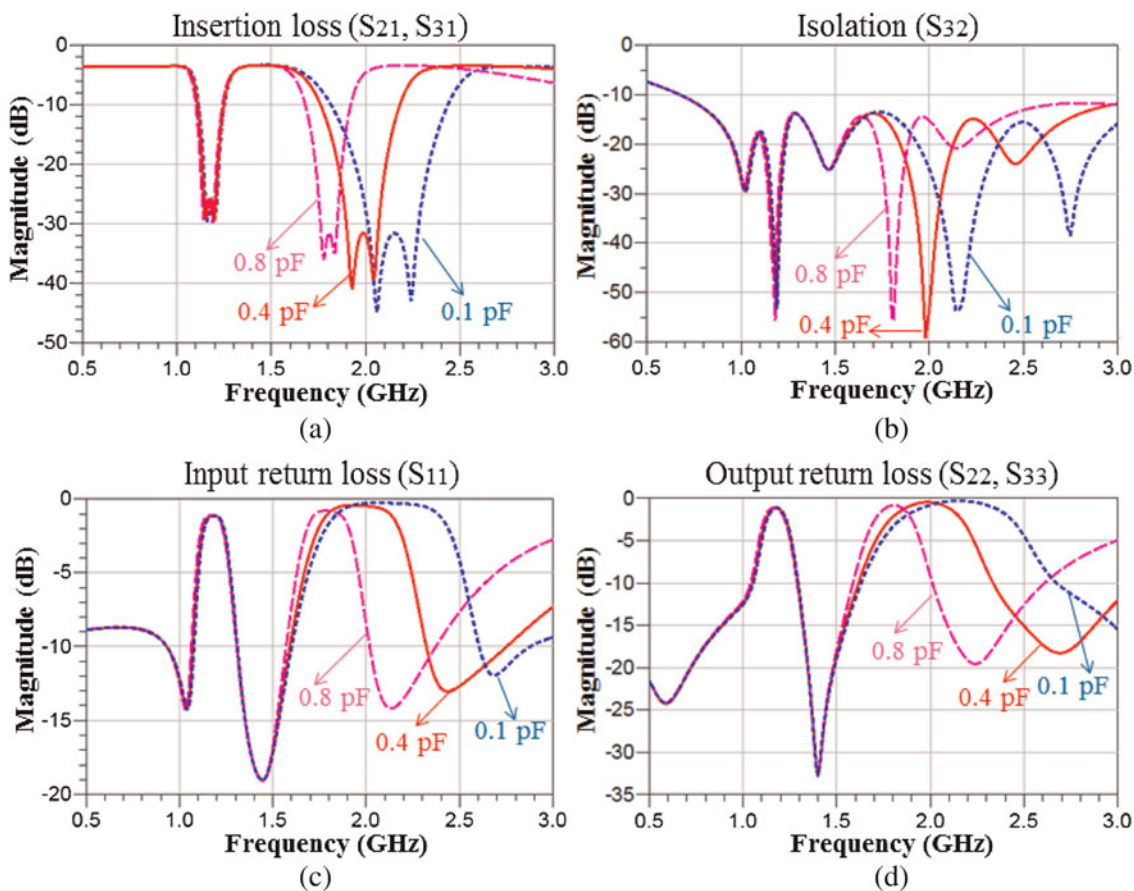
Fig. 8. Simulated comparison of the different capacitance values in the resonators f_1 in Fig. 7: (a) insertion loss of S_{21} and S_{31}, (b) isolation of S_{32}, (c) input return loss of S_{11}, (d) output return loss of S_{22} and S_{33}. Solid line, 0.4 pF; dot, 0.1 pF; and short dash, 0.8 pF.
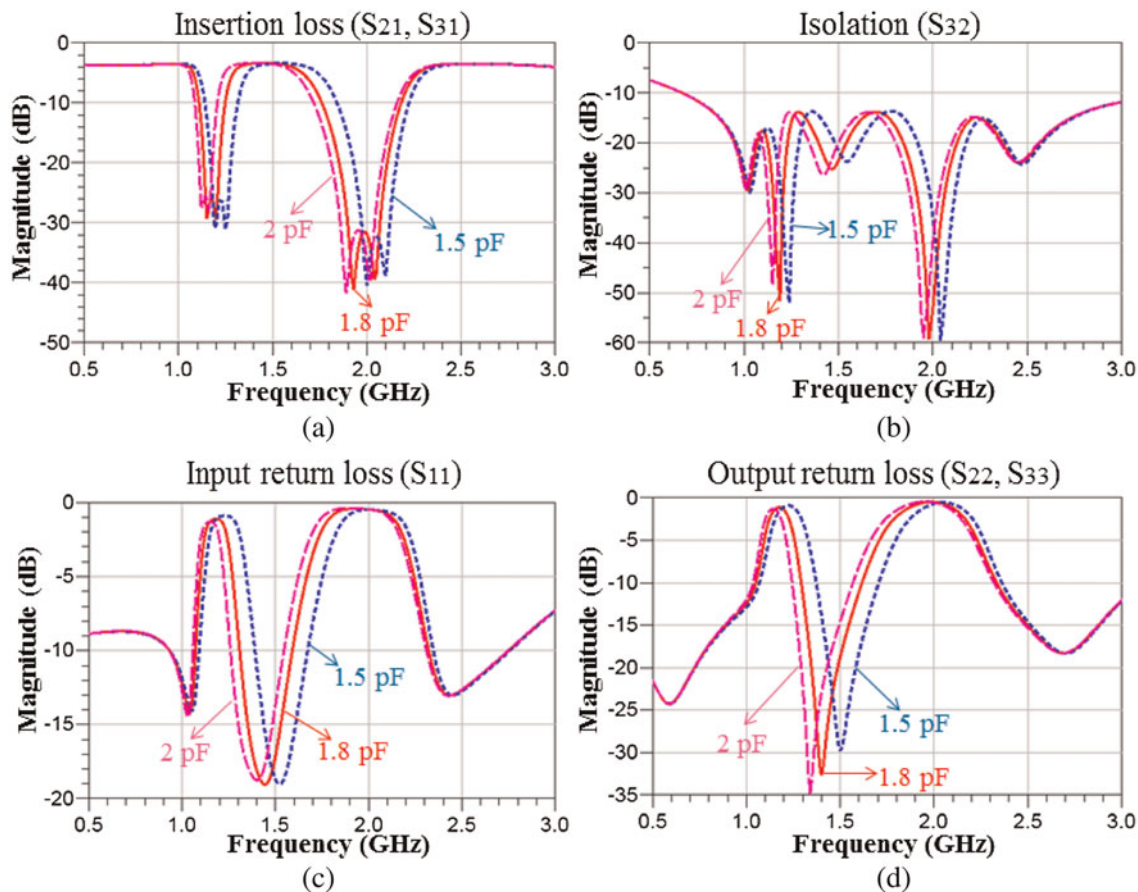
Fig. 9. Simulated comparison of the different capacitance values in the resonators f_2 in Fig. 7: (a) insertion loss of S_{21} and S_{31}, (b) isolation of S_{32}, (c) input return loss of S_{11}, (d) output return loss of S_{22} and S_{33}. Solid line, 1.8 pF; dot, 1.5 pF; and short dash, 2 pF.
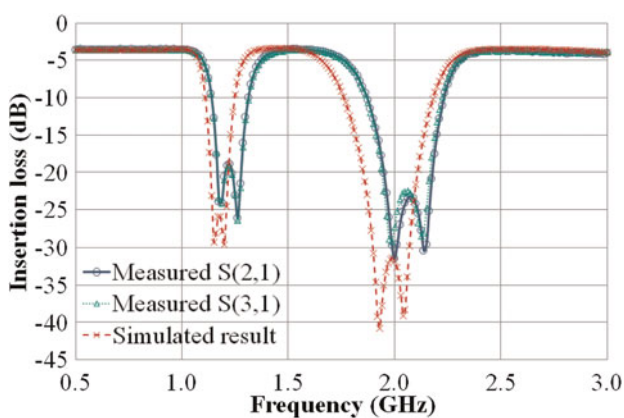

Fig. 10. Simulated (x) and measured (round and triangle) insertion loss of the tri-band Wilkinson power divider.
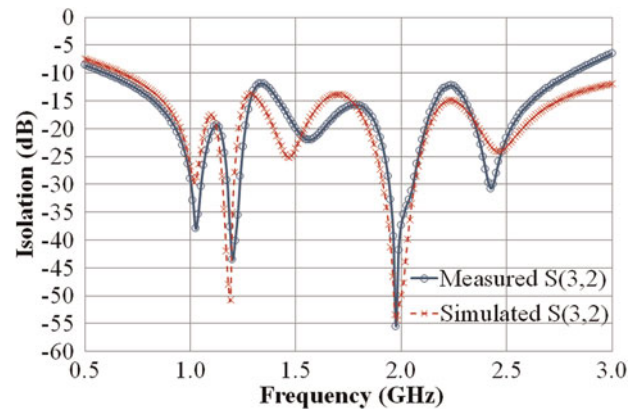

Fig. 11. Simulated (x) and measured (round) output port isolation of the tri-band Wilkinson power divider.

In Fig. 11, the measured isolation S_{32} at 1/1.5 /2.5 GHz is 29.05/19.93/21.65 dB.

In Fig. 12, the measured input return loss S_{11} at 1/1.5 /2.5 GHz is 12.29/13.56/14.49 dB.

In Fig. 13, the measured output return loss S_{22} and S_{33} at 1/1.5/2.5 GHz is 13.89/21.82/19.49 and 13.43/21.53/22.78 dB, respectively.

Comparing the simulated and measured results, there is a slight difference between them. The authors consider the

difference comes from the tolerance of the used components. For the used ATC 600S 0.4 pF capacitor, the tolerance is ± 0.1 pF; for the used ATC 600S 1.8 pF capacitor, the tolerance is ± 0.25 pF; for the used Coilcraft 0603 inductor, the tolerance is 2%.

The measured results of the tri-band Wilkinson power divider are summarized in Table 2.

The tri-band Wilkinson power divider in this work is compared with the work of Chongcheawchamnan et al. [10] as shown in Table 3. Chongcheawchamnan et al. [10] show a
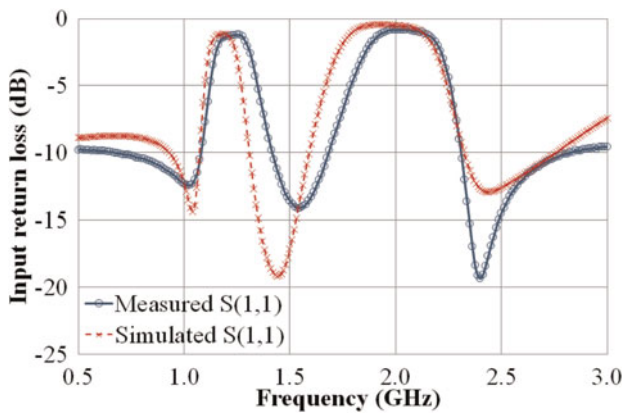
Fig. 12. Simulated (x) and measured (round) input return loss of the tri-band Wilkinson power divider.
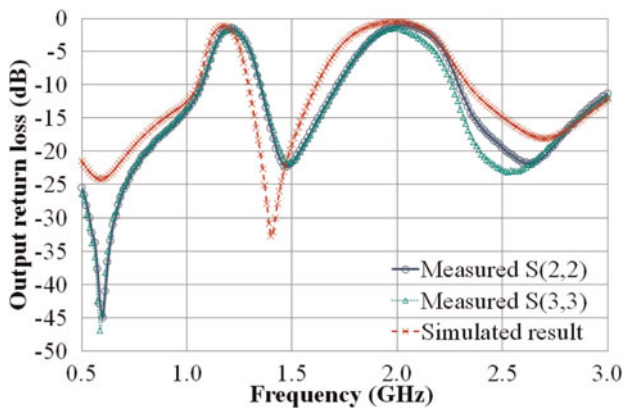

Fig. 13. Simulated (x) and measured (round and triangle) output return loss of the tri-band Wilkinson power divider.

tri-band Wilkinson power divider with the excellent and wideband performance. Being different from the reference, our work presents a relative narrow-band type and intrinsically

multiband Wilkinson power divider. The signal between the desired operating bands is well attenuated to avoid the potential interference between each operating frequency band. The proposed tri-band Wilkinson power divider in this work can be used for concurrent multiband PA applications. The size of the tri-band Wilkinson power divider in this work is 29 mm × 32 mm compared with the size of the power divider presented in [10] which is 31 mm × 55 mm. For the future work, the authors are considering increasing the operating frequency bandwidth by employing microstrip radial stub (MRS) according to its wideband characteristic [21].

B) Tri-band rat-race coupler

The topology and fabricated circuit of the proposed tri-band rat-race coupler are shown in Fig. 14. In the fabricated tri-band rat-race coupler, we used the thin MTL-type inductor instead of a chip inductor to avoid the limited standard inductance values provided by the manufacturers. To keep the compactness of the tri-band rat-race coupler, all stubs with resonators are putted inside the circuit itself.

In Fig. 14, the initial capacitance value of the capacitors in the resonators f_1 is 1.2 pF, and that of the capacitors in the resonators f_2 is 2.7 pF. The resonator f_1 composed of the chip capacitor and the MTL-type inductor has the resonant frequency of 2.5 GHz. Figures 15 and 16 show the simulated comparisons of only changing the capacitance value of the resonators f_1 in the tri-band rat-race coupler. By decreasing the capacitance value of the resonators f_1, the bandwidth of the middle operating frequency (1.5 GHz) can be increased and the highest operating frequency band (2.5 GHz) will shift to a higher band region. The resonators f_1 do not affect the performance of the lowest frequency band (1 GHz). Figures 17 and 18 show the simulated comparisons of only changing the capacitance value of the resonators f_2 in Fig. 14. The resonator f_2 has the resonant frequency of 1.5 GHz. It affects the performance of the middle operating

Table 2. Measured results of the tri-band Wilkinson power divider.

Freq. (GHz)	S21 (dB)	S31 (dB)	S32 (dB)	S11 (dB)	S22 (dB)	S33(dB)	∠S21 −∠S31 (°)
1	−3.58	−3.59	−29.05	−12.29	−13.89	−13.43	−0.28
1.5	−3.64	−3.64	−19.93	−13.56	−21.82	−21.53	−2.09
2.5	−3.78	−3.74	−21.65	−14.49	−19.49	−22.78	1.65
Design target	−3	−3	<−15	<−10	<−10	<−10	0

Table 3. Comparison between this work and the work of [10].

|	This work			Ref. [10]		
	Freq. (GHz)			Freq. (GHz)		
	1	1.5	2.5	0.9	1.17	2.43
S21 (dB)	−3.58	−3.64	−3.78	Better than −3.4	Better than −3.4	Better than −3.4
S31 (dB)	−3.59	−3.64	−3.74	Better than −3.4	Better than −3.4	Better than −3.4
S32 (dB)	−29.05	−19.93	−21.65	Better than −30	Better than −25	Better than −15
S11 (dB)	−12.29	−13.56	−14.49	Better than −30	Better than −30	Better than −25
S22 (dB)	−13.89	−21.82	−19.49	Better than −20	Better than −20	Better than −20
S33(dB)	−13.43	−21.53	−22.78	Better than −20	Better than −20	Better than −20
∠S21−∠S31 (°)	−0.28	−2.09	1.65	0.2	0.45	1.5
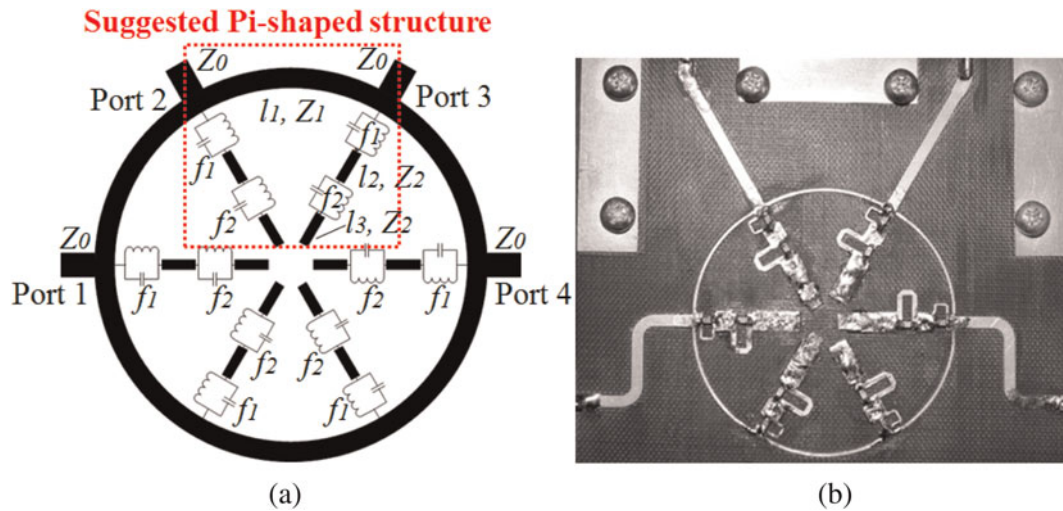
Fig. 14. The topology (a) and fabricated circuit (b) of the tri-band rat-race coupler.

frequency band (1.5 GHz). As Figs 17 and 18 show us, if the capacitance value of the resonators f_2 decreases, the middle operating frequency band (1.5 GHz) shifts to be higher, whereas the highest operating frequency band (2.5 GHz) being affected little. The final used capacitance values of the capacitors in the resonators f_1 and the resonators f_2 in the tri-band rat-race coupler are 1.2 and 2.7 pF, respectively.

The simulated and measured results of the fabricated tri-band rat-race coupler are compared from Figs 19–23. At 1/1.5/2.5 GHz, the measured results show that the insertion loss is less than 4.04 dB, the return loss is better than 10.16 dB; and the isolation between Ports 1 and 3, and Ports 2 and 4 are better than 26.09 and 22.13 dB, respectively. As shown in Fig. 24, in-phase difference $\angle S_{23} - \angle S_{43}$ is less than 2.32°, and out-of-phase difference $\angle S_{21} - \angle S_{41}$ is less than 183.84°. The measured results of the tri-band rat-race coupler in this paper are compared with the dual-band rat-race couplers proposed in [7, 8, 11] as shown in Table 5. The results are comparable. However, the proposed multiband design method in this paper is more general in terms of number of the operating frequency bands. As mentioned in the end of Section III(A), the authors are considering increasing the bandwidth of each operating frequency band by using MRS instead of using microstrip rectangular stub.
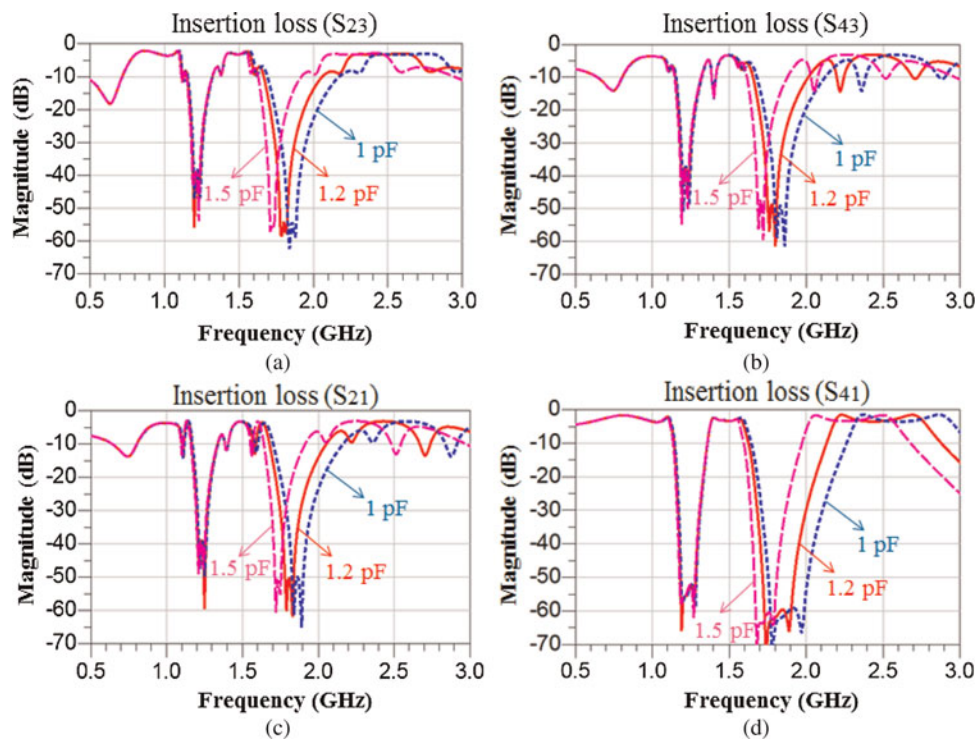

Fig. 15. Simulated comparison of insertion loss of using the different capacitance values in the resonators f_1 in Fig. 14, (a) S_{23}, (b) S_{43}, (c) S_{21}, (d) S_{41}. Solid line, 1.2 pF; dot, 1 pF; and short dash, 1.5 pF.
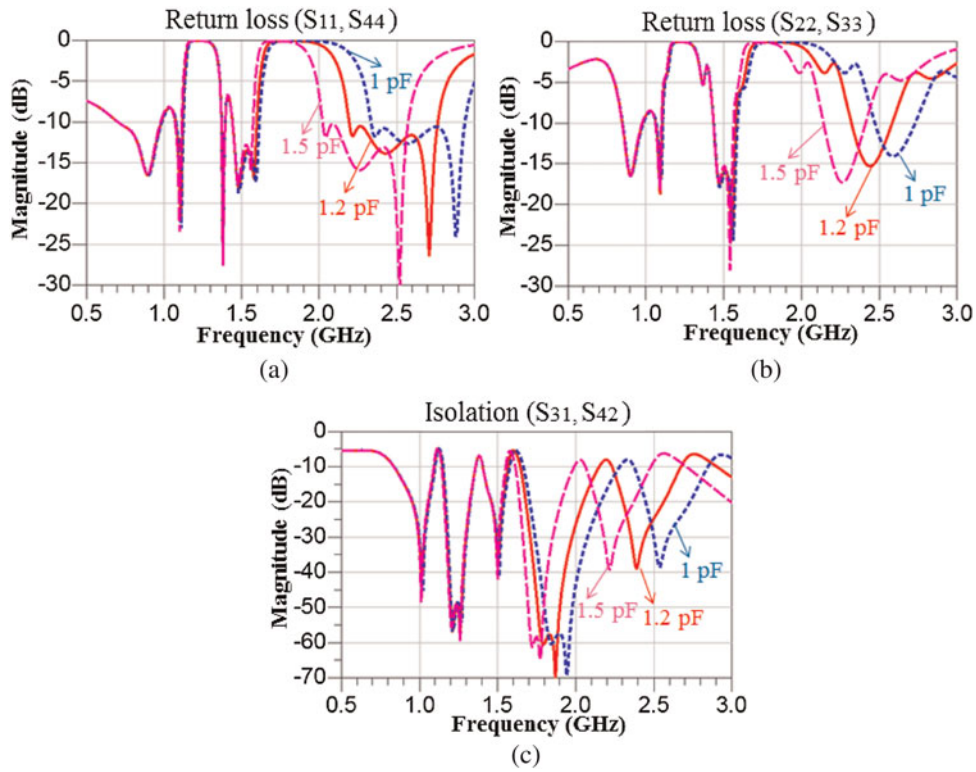
Fig. 16. Simulated comparison of return loss and isolation of using the different capacitance values in the resonators f_1 in Fig. 14: (a) S_{11} and S_{44}, (b) S_{22} and S_{33}, (c) S_{31} and S_{42}. Solid line, 1.2 pF; dot, 1 pF, and short dash, 1.5 pF.

In Fig. 19, the measured in-phase insertion loss S_{23} and S_{43} at 1/1.5 /2.5 GHz is 3.58/3.59/3.47 and 3.84/4.00/4.03 dB, respectively. The measured in-phase difference at 1/1.5/2.5 GHz is 1.02°/2.32°/1.14° as shown in Fig. 24 (dash).

In Fig. 20, the measured out-of-phase insertion loss S_{21} and S_{41} at 1/1.5/2.5 GHz is 3.77/3.87/3.92 and 3.88/4.04/3.87 dB, respectively. The measured out-of-phase difference at 1/1.5/2.5 GHz is 180.31°/183.84°/181.87° as shown in Fig. 24 (dot).
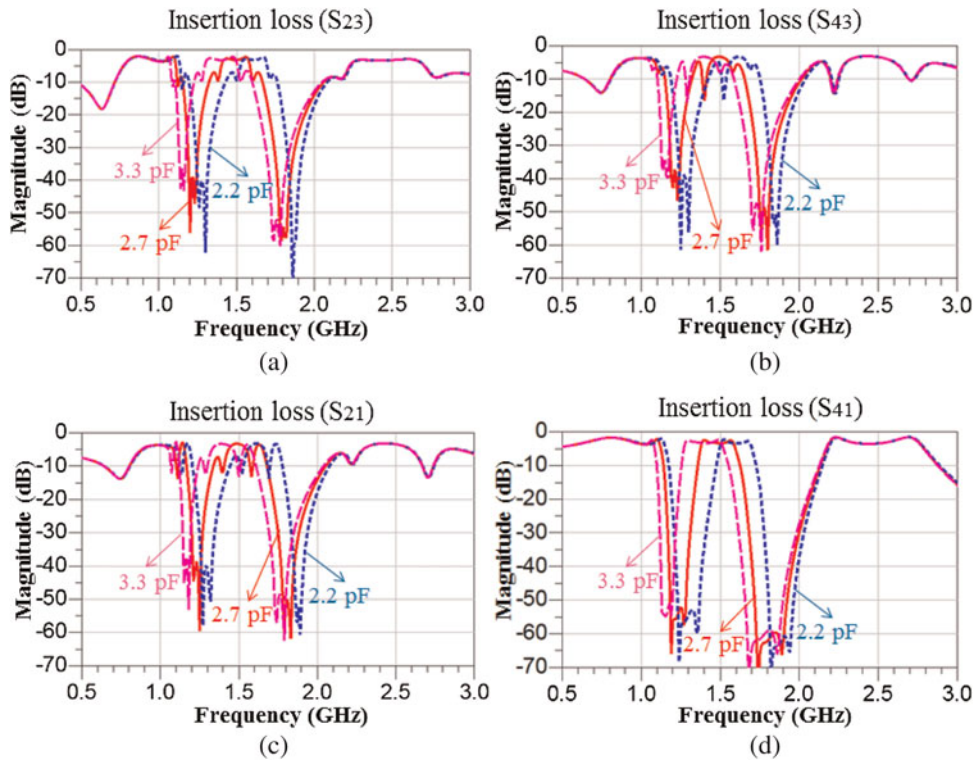

Fig. 17. Simulated comparison of insertion loss of using the different capacitance values in the resonators f_2 in Fig. 14: (a) S_{23}, (b) S_{43}, (c) S_{21}, (d) S_{41}. Solid line, 2.7 pF; dot, 2.2 pF; and short dash, 3.3 pF.
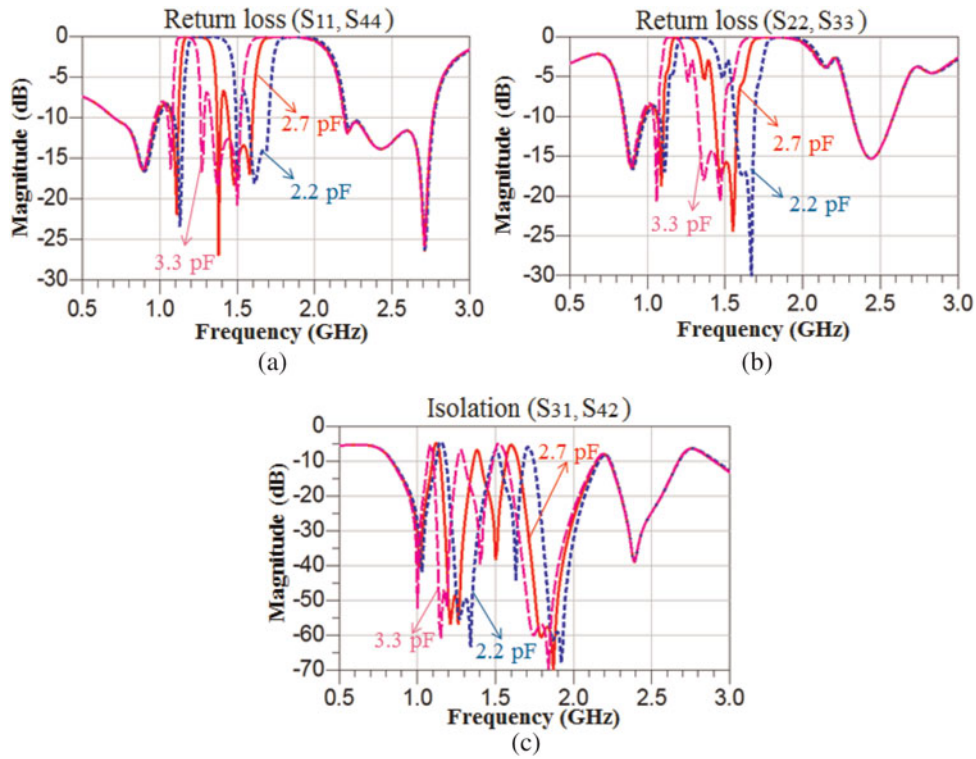
Fig. 18. Simulated comparison of return loss and isolation of using the different capacitance values in the resonators f_2 in Fig. 14: (a) S_{11} and S_{44}, (b) S_{22} and S_{33}, (c) S_{31} and S_{42}. Solid line, 2.7 pF; dot, 2.2 pF; and short dash, 3.3 pF.
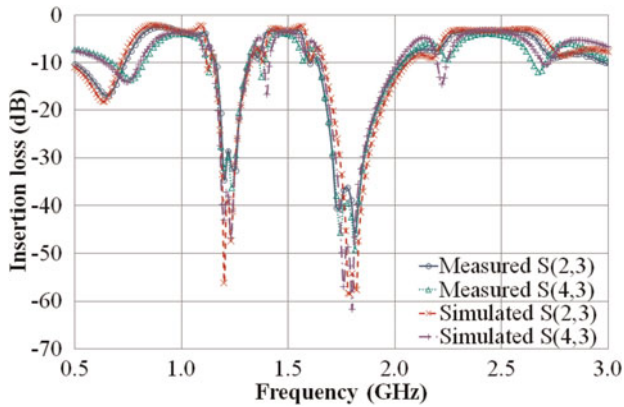

Fig. 19. Simulated (x and cross) and measured (round and triangle) insertion loss of S_{23} and S_{43} of the tri-band rat-race coupler.

Fig. 21. Simulated (x and cross) and measured (round and triangle) return loss of Ports 1 and 4 of the tri-band rat-race coupler.

Fig. 20. Simulated (x and cross) and measured (round and triangle) insertion loss of S_{21} and S_{41} of the tri-band rat-race coupler.
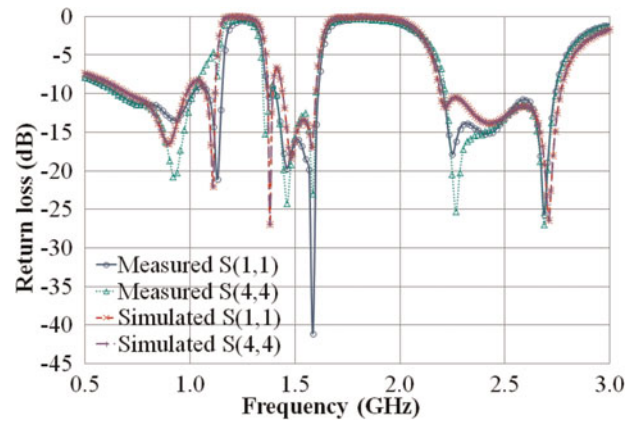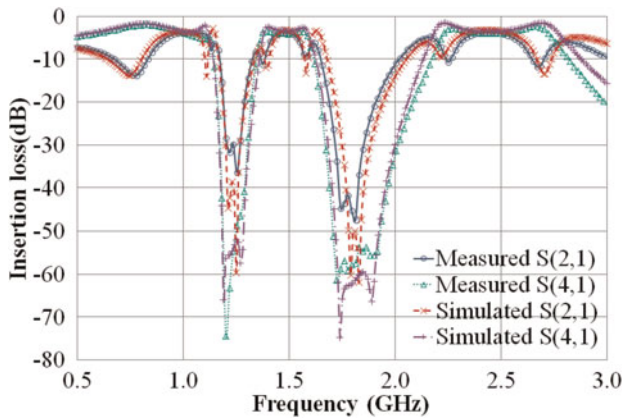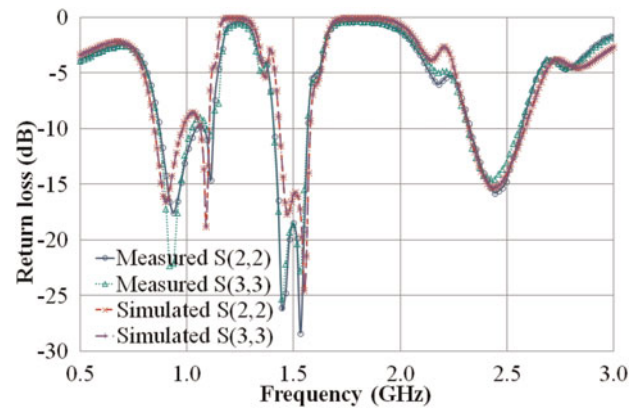

Fig. 22. Simulated (x and cross) and measured (round and triangle) return loss of Ports 2 and 3 of the tri-band rat-race coupler.
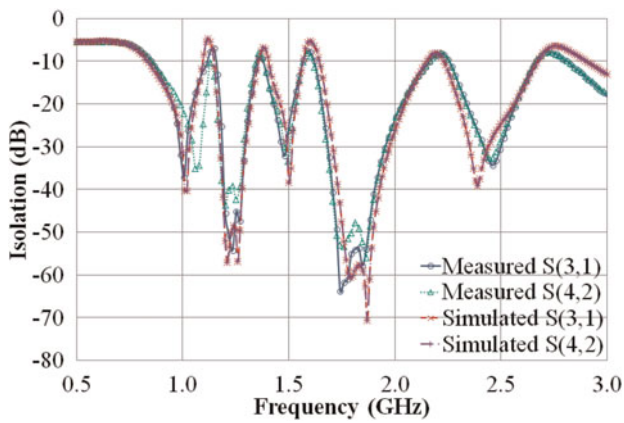
Fig. 23. Simulated (x and cross) and measured (round and triangle) isolation of S_{31} and S_{42} of the tri-band rat-race coupler.
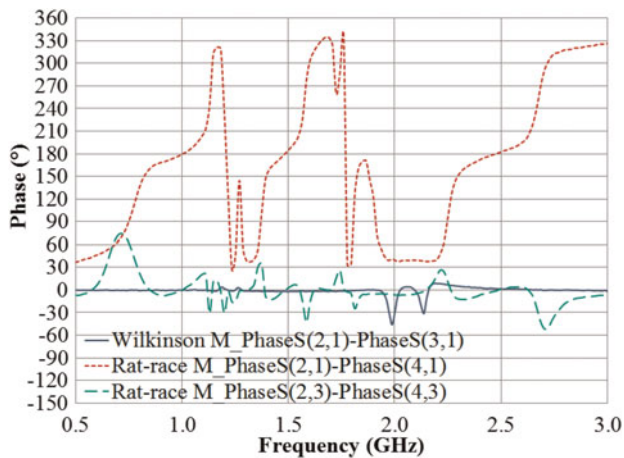

Fig. 24. Measured phase difference of output ports of the tri-band Wilkinson power divider (solid line) and tri-band rat-race coupler (dot and dash).

In Fig. 21, the measured return loss S_{11} and S_{44} at 1/1.5/2.5 GHz is 10.16/16.23/13.38 and 10.59/15.80/13.31 dB, respectively.

In Fig. 22, the measured return loss S_{22} and S_{33} at 1/1.5/2.5 GHz is 11.77/18.46/14.75 and 10.82/18.63/13.10 dB, respectively.

In Fig. 23, the measured isolation S_{31} and S_{42} at 1/1.5/2.5 GHz is 37.13/26.09/30.59 and 22.13/33.31/29.00 dB, respectively.

The measured results of the tri-band rat-race coupler are summarized in Tables 4 and 5.

IV. CONCLUSION

This paper presents a novel Pi-shaped structure for multiband applications. For the first time, the multiband (n-band, $n \geq 3$) Pi-shaped structure which is equal to multiband quarter wavelength TL has been investigated and analyzed by employing ABCD matrix. Resonators are used in the multiband Pi-shape structure to select operating frequency. This proposed Pi-shaped structure can be applied in multiband Doherty PA for its Wilkinson power divider and quarter wavelength TLs. To demonstrate the proposed multiband design method, at three frequencies 1/1.5/2.5 GHz, one tri-band Wilkinson power divider and one tri-band rat-race coupler are designed, fabricated, and tested. The compactness of the demonstrated circuits is kept by putting all stubs with resonators inside the circuits themselves. In addition, by choosing the series circuit element in the highest operating frequency, the total size of the demonstrated circuits is smaller than the single band circuit designed for the lower frequency. The excellence performance of the proposed multiband circuits is shown both by measurement and simulation. The multiband design method proposed in this paper can be widely applied in multiband applications.

Table 4. Measured results of tri-band rat-race coupler.

Freq. (GHz)	S_{23} (dB)	S_{43} (dB)	$\angle S_{23}-\angle S_{43}$ (°)	S_{21} (dB)	S_{41} (dB)	$\angle S_{21}-\angle S_{41}$ (°)	S_{11} (dB)	S_{44} (dB)	S_{22} (dB)	S_{33} (dB)	S_{31} (dB)	S_{42} (dB)
1	−3.58	−3.84	1.02	−3.77	−3.88	180.31	−10.16	−10.59	−11.77	−10.82	−37.13	−22.13
1.5	−3.59	−4.00	2.32	−3.87	−4.04	183.84	−16.23	−15.80	−18.46	−18.63	−26.09	−33.31
2.5	−3.47	−4.03	1.14	−3.92	−3.87	181.87	−13.38	−13.31	−14.75	−13.10	−30.59	−29.00
Design target	−3	−3	0	−3	−3	180	<−10	<−10	<−10	<−10	<−15	<−15

Table 5. Comparison between this work and the works of [7], [8], and [11].

	This work			Ref.[7]		Ref.[8]		Ref.[11]	
	Freq. (GHz)			Freq. (GHz)		Freq. (GHz)		Freq. (GHz)	
	1	1.5	2.5	1.544	3.043	2.4	5.2	2.34	5
In-phase insertion loss (dB)	3.84	4.00	4.03	–	–	4.04	4.53	3.48	4.22
In-phase phase difference (°)	1.02	2.32	1.14	–	–	4.3	1.9	1.12	2.07
Out-of-phase insertion loss (dB)	3.88	4.04	3.92	4.126	4.065	–	–	–	–
Out-of-phase phase difference (°)	180.31	183.84	181.87	176.20	182.24	–	–	181.48	179.1
Isolation (dB) (S_{31}, S_{42})	22.13	26.09	29.00	31.003	32.857	29.97	22.11	29.6	43.21
Return loss (dB) (S_{11}, S_{44})	10.16	15.80	13.31	12.185	22.524	–	–	–	–
Return loss (dB) (S_{22}, S_{33})	10.82	18.46	13.10	–	–	19.62	23.39	20.86	18.08

REFERENCES

[1] Wang, C.Y.; Lu, S.S.; Meng, C.C.; Lin, Y.S.: A GaInP/GaAs HBT micromixer for 2.4/5.2/5.7-GHz multiband WLAN applications. Microw. Opt. Technol. Lett., **43** (1) (2004), 87–89.

[2] Yuan, Z.-X.; Yin, Y.-Z.; Ding, Y.; Li, B.; Xie, J.J.: Multiband printed and double-sided dipole antenna for WLAN/WiMAX applications. Microw. Opt. Technol. Lett., **54** (4) (2012), 1019–1022.

[3] Herbertz, K.; Lucyszyn, S.: Two-dimensional metamaterials for dual-band filter applications, in 38th European Microwave Conf., Amsterdam, The Netherlands, 2008.

[4] Tseng, C.-H.; Shao, H.-Y.: A new dual-band microstrip bandpass filter using net-type resonators. IEEE Microw. Wirel. Compon. Lett., **20** (4) (2010), 196–198.

[5] Park, M.-J.: Two-section cascaded coupled line Wilkinson power divider for dual-band applications. IEEE Microw. Wirel. Compon. Lett., **19** (4) (2009), 188–190.

[6] Wu, Y.; Liu, Y.; Zhang, Y.; Gao, J.; Zhou, H.: A dual band unequal Wilkinson power divider without reactive components. IEEE Trans. Microw. Theory Tech., **57** (1) (2009), 216–222.

[7] Lin, I.-H.; DeVincentis, M.; Caloz, C.; Itoh, T.: Arbitrary dual-band components using composite right/left-handed transmission lines. IEEE Trans. Microw. Theory Tech., **52** (4) (2004), 1142–1149.

[8] Chi, P.-L.; Lee, C.-J.; Itoh, T.: A compact dual-band metamaterial-based rat-race coupler for a MIMO system application, in IEEE MTT-S Int. Microwave Symp. Digest, Atlanta, USA, 2008.

[9] Chiou, Y.-C.; Kuo, J.-T.; Chan, C.-H.: New miniaturized dual-band rat-race coupler with microwave C-section, in IEEE MTT-S Int. Microwave Symp. Digest, Boston, USA, 2009.

[10] Chongcheawchamnan, M.; Patisang, S.; Krairiksh, M.; Robertson, I.D.: Tri-band Wilkinson power divider using a three-section transmission-line transformer. IEEE Microw. Wirel. Compon. Lett., **16** (8) (2006), 452–454.

[11] Chin, K.-S.; Lin, K.-M.; Wei, Y.-H.; Tseng, T.-H.; Yang, Y.-J.: Compact dual-band branch-line and rat-race couplers with stepped-impedance-stub lines. IEEE Trans. Microw. Theory Tech., **58** (5) (2010), 1213–1221.

[12] Edmund Neo, W.C. et al.: Adaptive multi-band multi-mode power amplifier using integrated varactor-based tunable matching networks. IEEE J. Solid-State Circuits, **41** (9) (2006), 2166–2176.

[13] Fukuda, A.; Okazaki, H.; Hirota, T.; Yamao, Y.: Novel 900 MHz/ 1.9 GHz dual-mode power amplifier employing MEMS switches for optimum matching. IEEE Microw. Wirel. Compon. Lett., **14** (3) (2004), 121–123.

[14] Hur, J.; Lee, O.; Lee, C.-H.; Lim, K.; Laskar, J.: A multi-level and multi-band class-D CMOS power amplifier for the LINC system in the cognitive radio application. IEEE Microw. Wirel. Compon. Lett., **20** (6) (2010), 352–354.

[15] Kalim, D.; Negra, R.: Concurrent planar multiharmonic dual-band load coupling network for switching-mode power amplifiers, in IEEE MTT-S Int. Microwave Symp. Digest, Baltimore, USA, 2011.

[16] Wang, Z.; Park, C.-W.: Dual-band GaN HEMT power amplifier using resonators in matching networks, in 12th Annual IEEE Wireless and Microwave Technology (WAMI) Conf., Clearwater, USA, 2011.

[17] Wang, Z.; Park, C.-W.: Concurrent tri-band GaN HEMT power amplifier using resonators in both input and output matching networks, in 13th Annual IEEE Wireless and Microwave Technology (WAMI) Conf., Cocoa Beach, USA, 2012.

[18] Kim, I.; Moon, J.; Kim, J.; Jee, S.; Son, J.; Kim, B.: High efficiency 3-stage Doherty power amplifier using gate bias adaption. Int. J. Microw. Wirel. Technol., **3** (1) 2011, 47–58.

[19] Wang, Z.; Park, C.-W.: Multiband Pi-shaped structure with resonators for tri-band Wilkinson power divider and tri-band rat-race coupler, in IEEE MTT-S Int. Microwave Symp. Digest, Montreal, Canada, 2012.

[20] Pozar, D.M.: 5.4 The quarter-wave transformer, In Microwave Engineering, 4th ed., John Wiley & Sons, Inc., USA, 2012, 246–247.

[21] Wang, Z.; Park, C.-W.: Novel wideband GaN HEMT power amplifier using microstrip radial stub to suppress harmonics, in IEEE MTT-S Int. Microwave Symp. Digest, Montreal, Canada, 2012.

Zhebin Wang was born in Nantong, Jiangsu province, China. He received the B.Sc. degree from Nanjing University of Information Science & Technology (NUIST), Jiangsu, China, in 2008. He obtained the M.Sc. degree in Electrical Engineering from University of Quebec in Rimouski (UQAR), Quebec, Canada, in 2013. His research interests are high-efficiency power amplifiers and circuits for multiband applications. In 2012, he won the second place in the "2012 IEEE MTT-S International Microwave Symposium Student High Efficiency Power Amplifier Design Competition" in IEEE MTT-S International Microwave Symposium (IMS2012) hold in Montreal, Canada.

Chan-Wang Park has received the B.Sc. degree in Electronic and Communication Engineering from Han Yang University, in Seoul, Korea in 1981 and M.Sc. degree from E.N.S.T. de Paris in France and Ph.D. degree from IEMN, Université des sciences et technologies de Lille 1 in France 1996 and 2001, respectively. From 1981 to 1985 he was in R&D center with Gold Star Electric (L.G. Telecom) at AnYang in Korea. From 1985 to 1990 he was in Training Centre in Saudi Telecom as a Technical Instructor. From 1990 to 1994 he developed three satellites at Satellite Technology Research Centre in KAIST, in Korea as a project manager. From 1994 to 1995 he was with IAS and Matra Marconi Space in France. From 2001 to 2002 he was with AmpliX and Mitec Telecom in Canada. In 2003, he joined the Université du Québec à Rimouski, where he is currently a professor. His research area is high power amplifier design, a characterization of transistor and RF/microwave and millimeter wave components design.